

1N-52-CR  
77021  
P 13

MCAT Institute  
Final Report 92-003

---

# INCOMPRESSIBLE VISCOUS FLOW COMPUTATIONS FOR THE PUMP COMPONENTS AND THE ARTIFICIAL HEART

---

Dr. Cetin Kiris

---

March 1992

NCC2-500

(NASA-CR-190076) INCOMPRESSIBLE VISCOUS  
FLOW COMPUTATIONS FOR THE PUMP COMPONENTS  
AND THE ARTIFICIAL HEART Final Report (MCAT  
Inst.) 13 p CSCL 06C

N92-20668

Unclas  
G3/52 0077021

MCAT Institute  
3933 Blue Gum Drive  
San Jose, CA 95127

*CASI*

MCAT Institute  
Final Report 92-003

---

# **INCOMPRESSIBLE VISCOUS FLOW COMPUTATIONS FOR THE PUMP COMPONENTS AND THE ARTIFICIAL HEART**

---

Dr. Cetin Kiris

---

March 1992

NCC2-500

**MCAT Institute  
3933 Blue Gum Drive  
San Jose, CA 95127**

# COMPUTATION OF INCOMPRESSIBLE VISCOUS FLOWS THROUGH TURBOPUMP COMPONENTS

Cetin Kiris

ORIGINAL DOCUMENT  
COLOR REPRODUCTION

## Abstract

A finite-difference, three dimensional incompressible Navier-Stokes formulation to calculate the flow through turbopump components is utilized. The solution method is based on the pseudocompressibility approach and uses an implicit-upwind differencing scheme together with the Gauss-Seidel line relaxation method. Both steady and unsteady flow calculations can be performed using the current algorithm. In this work, the equations are solved in steadily rotating reference frames by using the steady-state formulation in order to simulate the flow through a turbopump inducer. Eddy viscosity is computed by using an algebraic mixing-length turbulence model. Numerical results are compared with experimental measurements and a good agreement is found between the two. Time-accurate calculations, such as impeller and diffuser interaction, will be reported in future work.

## Introduction

With the advent of supercomputer hardware as well as fast numerical methods, computational fluid dynamics (CFD) has become an essential part of aerospace research and design. Numerical studies in incompressible flows show good progress in parallel with computational studies in compressible flows. For example, the incompressible flow solver developed by Kwak et al [1] was extensively used for simulating the flow through space shuttle main engine power head components. The redesign of the space shuttle main engine hot gas manifold, guided by the computations of Chang et al. [2], illustrates the usefulness of CFD in aerospace research. Since the incompressible Navier-Stokes formulation does not yield the pressure field explicitly from the equation of state or through the continuity equation, numerical solution of the equations requires special attention in order to satisfy the divergence-free constraint on the velocity field. The most widely used methods which use primitive variables are fractional-step and pseudocompressibility techniques. In the fractional-step method, the auxiliary velocity field is solved by using the momentum equations. Then, a Poisson equation for pressure is formed by taking the divergence of the momentum equations and by using a divergence-free velocity field constraint. Solving the Poisson equation for pressure efficiently in three-dimensional curvilinear coordinates is the most important feature of the fractional step method.<sup>3</sup> One way to avoid the numerical difficulty originated by the elliptic nature of the problem is to use a pseudocompressibility method. With the pseudocompressibility method, the elliptic-parabolic type equations are transformed

into hyperbolic-parabolic type equations. Well established solution algorithms developed for compressible flows can be utilized to solve the resulting equations.

Steger and Kutler<sup>4</sup> employed an alternating direction implicit scheme into Chorin's<sup>5</sup> pseudocompressibility method. This formulation was extended to three-dimensional generalized coordinates by Kwak.<sup>1</sup> Recently, a three-dimensional incompressible Navier-Stokes solver (INS3D-LU-SGS) using a lower-upper symmetric-Gauss-Seidel algorithm was developed by Yoon and Kwak.<sup>6</sup> This algorithm is used to calculate the inducer flow of the Space Shuttle Main Engine turbopump in order to demonstrate the performance of the numerical method.<sup>7</sup> Another effort is performed in Ref. 8 by using upwind differencing and Gauss-Seidel line relaxation scheme in order to have a robust and fast converging scheme (INS3D-UP). A time accurate formulation of this algorithm is implemented for incompressible flows through artificial heart devices with moving boundaries.<sup>8,10</sup> In the present study, the steady-state formulation is used in steadily rotating reference frames in order to develop a CFD procedure for simulating the flow through turbopump components of a liquid rocket engine.

## Computed Results

The flowfield through a turbopump inducer is solved as a benchmark problem in order to validate the CFD procedure for turbomachinery applications. In this section results obtained for the Rocketdyne inducer shown in Fig. 1 are presented. The inducer geometry was developed and experimentally studied by the Rocketdyne Division of Rockwell International. The design flow is 2236 GPM with a design speed of 3600 RPM. In the computational study, tip-leakage effects are included with a tip clearance of 0.008 inches. The problem was nondimensionalized with a tip diameter of 6.0 inches and the average inflow velocity of 28.3 ft/sec. The Reynolds number for this calculation was 191,800. The upstream section of the inducer was taken as a two tip-diameter-long straight channel, as shown in Fig. 1. The bull-nose of the inducer was treated as a rotating wall and the cavity section was neglected. However, this region can be included by using an additional zone. An H-H grid topology with dimensions of 187 x 27 x 35 was used. A partial view of the surface grid is shown in Fig. 2. An H-type surface grid was generated for each surface using an elliptic grid generator. The interior region of the three-dimensional grid was filled using an algebraic solver coupled with an elliptic smoother. In the straight channel, the grid was generated for one-sixth of the cross-section of the tube. This grid was extended to the outflow section of the inducer between the blades. Periodic boundary conditions were used at the end points in the rotational direction. At inflow and outflow boundaries characteristic boundary conditions were employed. At the inflow,  $v$  and  $w$  velocity components were specified as zero and the total pressure was specified as constant. Axial velocity and static pressure were calculated from the characteristic relation and the total pressure relation. At the outflow, static pressure was specified and the velocity components were computed from the characteristics propagating from the interior region. The flow was taken at rest initially and the inducer was fully rotated impulsively. The solution was considered converged when the maximum residual dropped at least four orders of magnitude. This

was obtained in less than 500 iterations. Computer time required per grid point per iteration was about  $1.4 \times 10^{-4}$  sec.

Figure 3 illustrates the planes where the experimental measurements were taken by Rocketdyne. Axial and tangential velocity components and the flow angle were measured in planes A,B,C and D at various circular arcs from the hub to the tip region. At each plane, the comparison between experimental measurements and numerical results along three of the circular arcs is presented in this paper. A total velocity and a flow angle are compared against experimental data. The total velocity has only a tangential and an axial velocity components. The radial velocity component was not measured in the experiment.

Figures 4 through 7 show relative total velocities and relative flow angles as a function of circumferential angle in degrees in planes A, B, C, and D, respectively. The circumferential angle increases from the suction side to the pressure side. The dashed lines in these figures represent the experimental data and solid lines represent the numerical results. The comparison of computations and experiment is generally good all the way from the hub to tip region. The difference between experimental and numerical data is about 5-8 % in velocity. In all planes, the hub and tip regions indicate the biggest discrepancy. This may be a result of the relatively coarse grid used for the boundary layer. In the computational study, the Baldwin-Lomax algebraic turbulence model is used to determine the eddy viscosity. The comparison shows that the solution algorithm does a good job with an algebraic turbulence model. The implementation of the one equation model<sup>11</sup> of Baldwin and Barth is currently underway for the present algorithm. The motivation for higher-order turbulence modeling is due to the comparisons obtained in Plane D, in which the wake region is not predicted accurately (Fig. 7). Another advantage of the one-equation model is that there is no need to define a length-scale explicitly. Near the tip clearance region, the difference between experimental measurements and numerical results is noticeably larger than the error in other regions. This is due to lack of grid resolution in the tip clearance region. In the grid refinement study, the number of grid points in the tip clearance region was increased from 4 points to 9 points. In the coarse grid computation, there is one overlapped grid point in the rotational direction to ensure periodic boundary conditions. In the fine grid, additional 3 zones were added in radial direction. The results with the one equation model and the results from the grid refinement study will be published in future.

Figure 8 shows the surface of the inducer colored by nondimensionalized pressure. The pressure gradient across the blades due to the action of centrifugal force and the pressure rise from inflow to outflow are illustrated. This pressure rise along the inducer can also be seen in Fig. 9. Velocity vectors are plotted in the meridional plane and the vectors are colored by the static pressure. The existing solution procedure can be applied to the same configuration under off-design conditions. The massive separation which may block the fuel supply can be detected in the numerical study. This is the future research area of the present study which can be used as a pre-design and post-design engineering tool in challenging turbomachinery applications.

## Summary

An efficient and robust solution procedure is implemented and validated for three-dimensional turbopump applications. Numerical simulations of the flow through the Rocketdyne inducer have been successfully carried out by using CFD techniques for solving viscous incompressible Navier-Stokes equations with the source terms in steadily rotating reference frames. The method of artificial compressibility with a higher-order accurate upwind differencing and the Gauss-Seidel line relaxation scheme provide fast convergence and robustness. Results in the form of relative total velocity and relative flow angle in four planes are presented. Numerical results compare fairly well with experimental data.

## References

- <sup>1</sup> Kwak, D., Chang, J. L. C., Shanks, S. P., and Chakravarthy, S., "A Three-Dimensional Incompressible Navier-Stokes Flow Solver Using Primitive Variables", *AIAA Journal*, Vol 24, no. 3, pp. 390-396, 1977.
- <sup>2</sup> Chang, J. L. C., Kwak, D., Rogers, S. E., and Yang, R.-J., "Numerical Simulation Methods of Incompressible Flows and an Application to the Space Shuttle Main Engine", *Int. J. Num. Meth. in Fluids*, Vol 8, pp. 1241-1268, 1988.
- <sup>3</sup> Rosenfeld, M., Kwak, D. and Vinokur, M., "A Fractional Step Solution Method for the Unsteady Incompressible Navier-Stokes Equations in Generalized Coordinate Systems", to appear *Journal of Computational Physics*, 1991.
- <sup>4</sup> Steger, J. L., Kutler, P., "Implicit Finite-Difference Procedures for the Computation of Vortex Wakes", *AIAA Journal*, Vol 15, no. 4, pp. 581-590, Apr. 1977.
- <sup>5</sup> Chorin, A., J., "A Numerical Method for Solving Incompressible Viscous Flow Problems", *Journal of Computational Physics*, vol. 2, pp. 12-26, 1967
- <sup>6</sup> Yoon, S., Kwak, D., "Three-Dimensional Incompressible Navier-Stokes Solver Using Lower-Upper Symmetric-Gauss-Seidel Algorithm", *AIAA Journal*, Vol 29, No 4, pp. 874-875, 1991
- <sup>7</sup> Yoon, S., Kwak, D., "Implicit Methods for the Navier-Stokes Equations", *Computing Systems in Engineering*, Vol 1, Nos 2-4, pp. 535-547, 1990
- <sup>8</sup> Rogers, S. E., Kwak, D. and Kiris, C., "Numerical Solution of the Incompressible Navier-Stokes Equations for Steady and Time-Dependent Problems", *AIAA Journal*, Vol 29, No 4, pp. 603-610, 1991
- <sup>9</sup> Kiris, C., Chang, I., Rogers, S. E. and Kwak, D., "Numerical Simulation of the the Incompressible Internal Flow Through a Tilting Disk Valve", AIAA Paper 90-0682, 1990.
- <sup>10</sup> Kiris, C., Rogers, S. E., Kwak, D. and Chang, I. "Computation of Incompressible Viscous Flows with Moving Boundaries", Proc. Intl. Symposium on Biofluidynamics, July 6-12, 1991.
- <sup>11</sup> Baldwin, B., S. and Barth, T., J., "A One-Equation Turbulence Transport Model for High Reynolds Number Wall-Bounded Flows", AIAA Paper No. 91-0610, 1991.

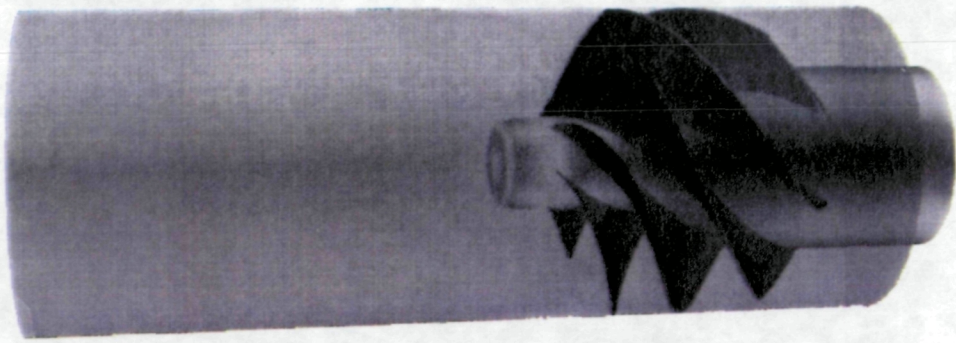


Figure 1: Rocketdyne turbopump inducer configuration.

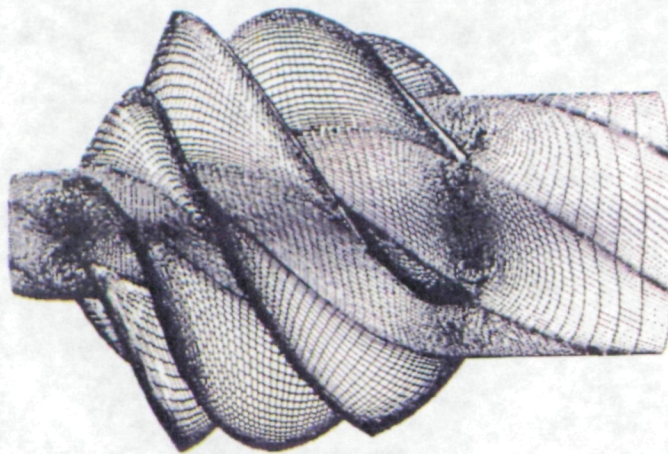


Figure 2: Surface grid for Rocketdyne turbopump inducer.

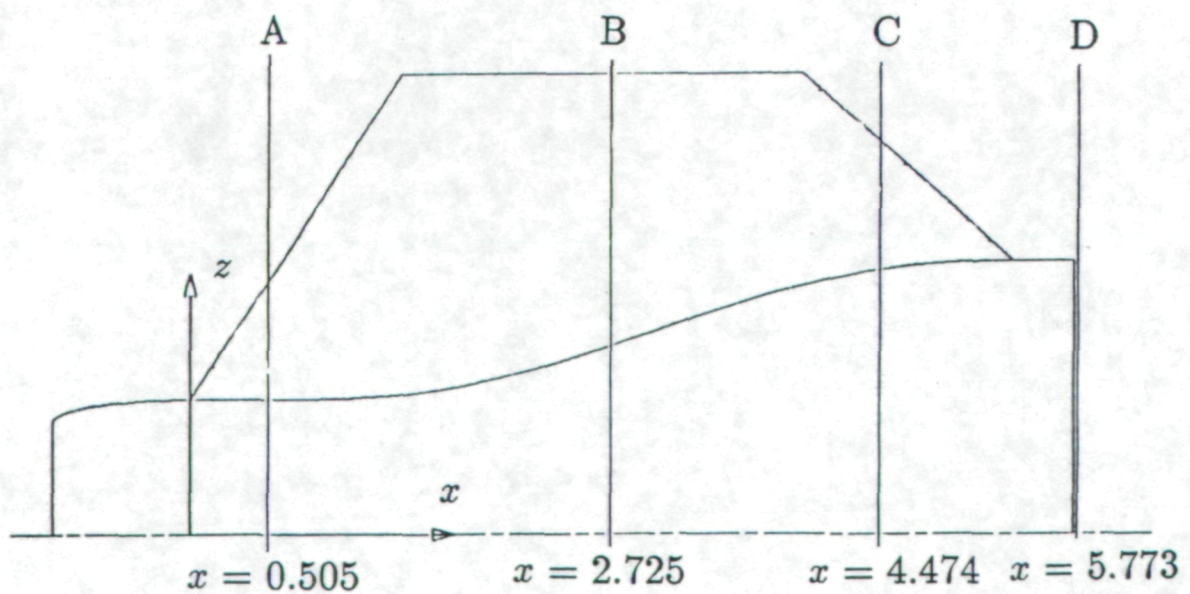
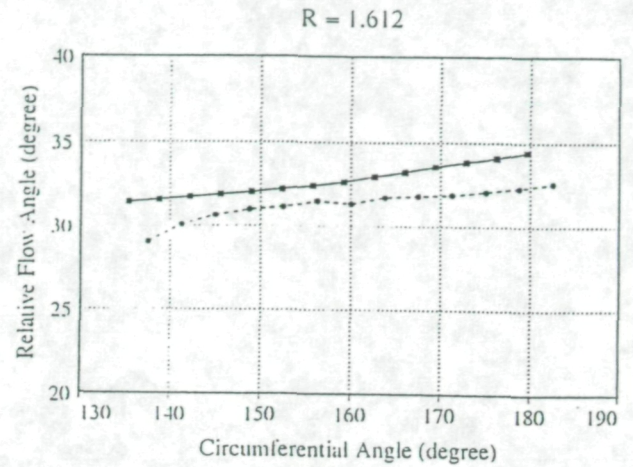
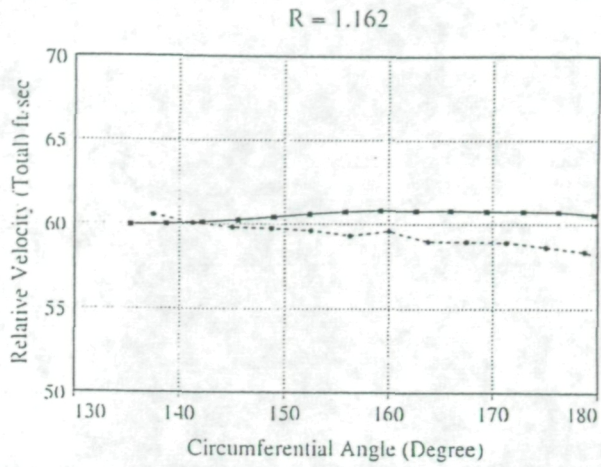


Figure 3: Schematic representation of the planes where experimental data is available.



-●- Experiments  
 -■- Computations

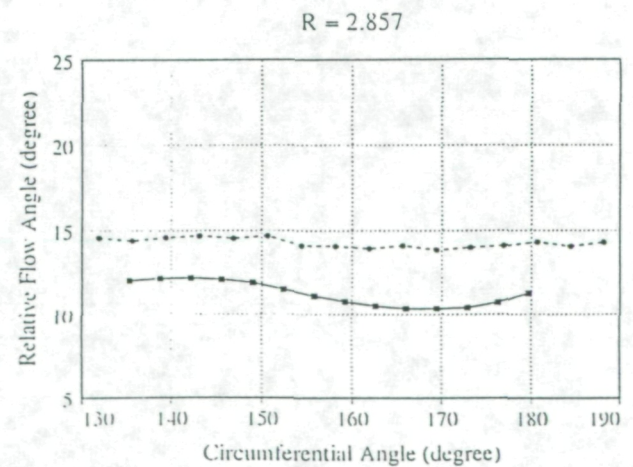
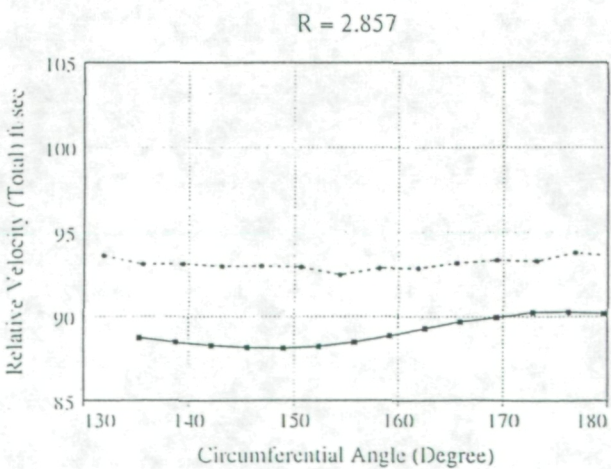
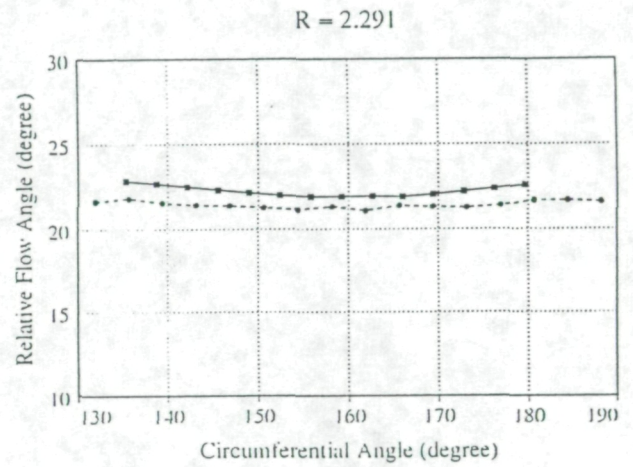
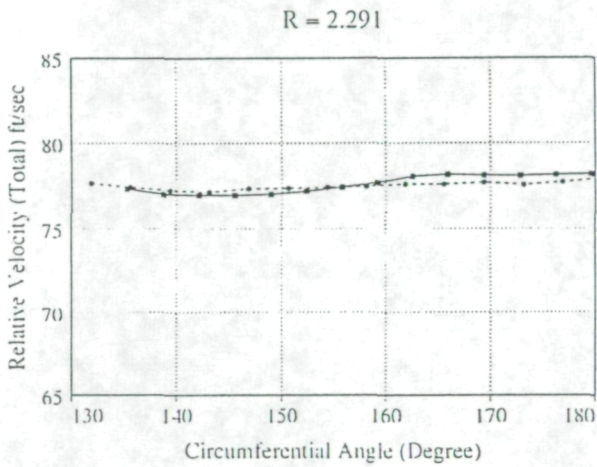


Figure 4: Comparison of relative total velocity and relative flow angle in Plane A.



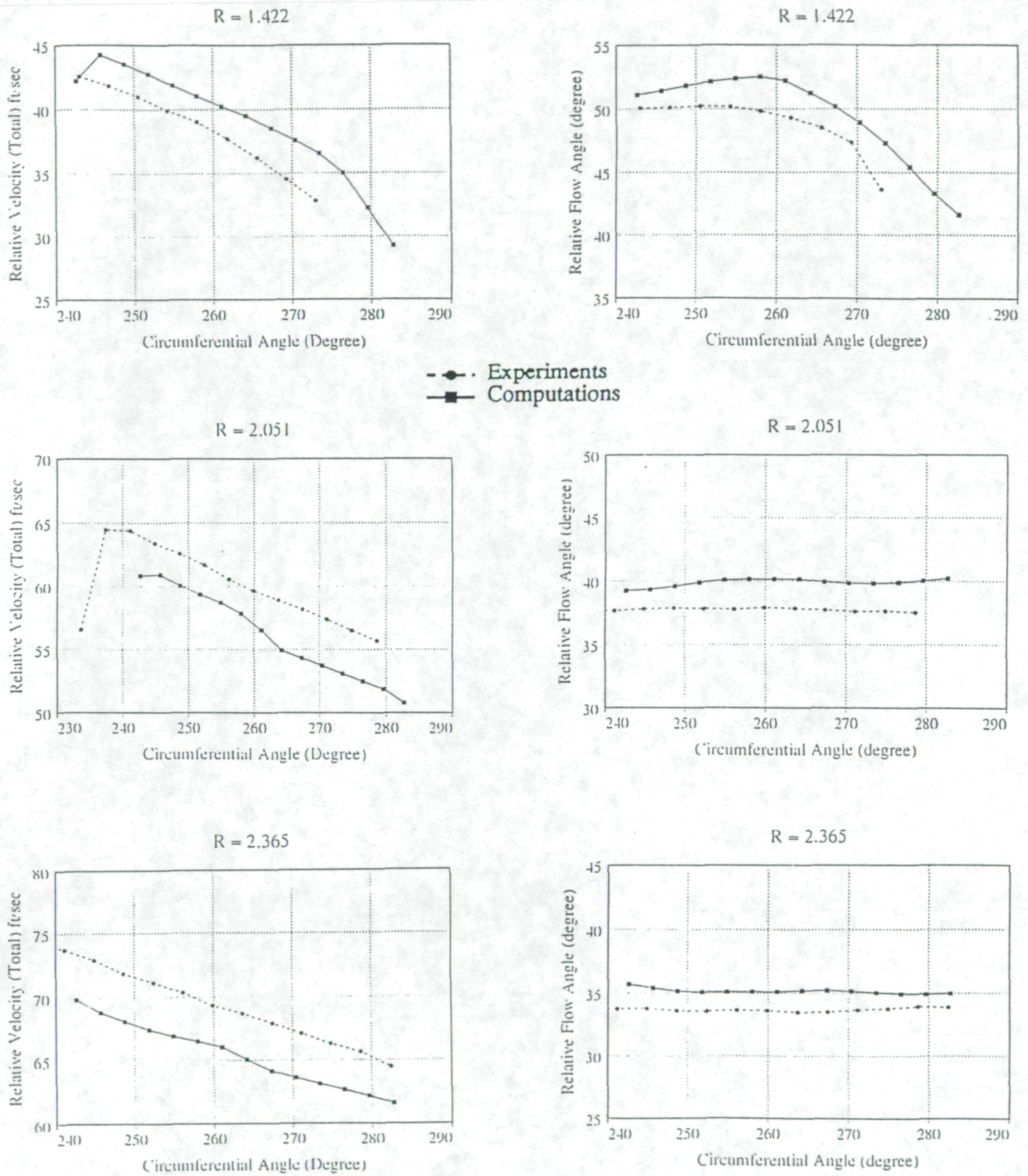
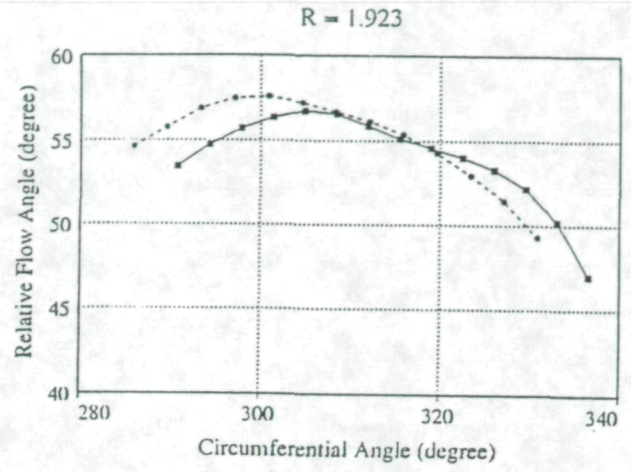
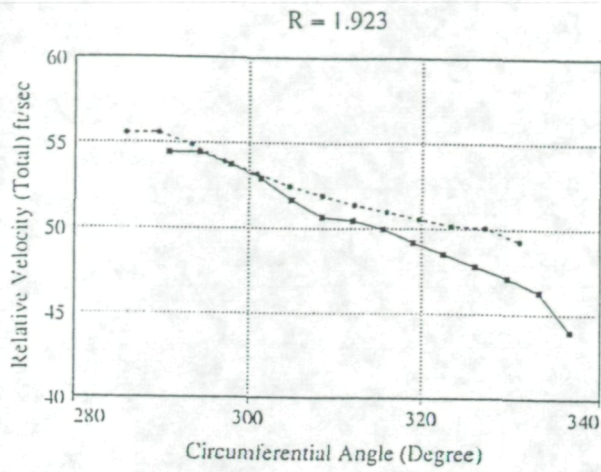


Figure 5: Comparison of relative total velocity and relative flow angle in Plane B.



-●- Experiments  
 -■- Computations

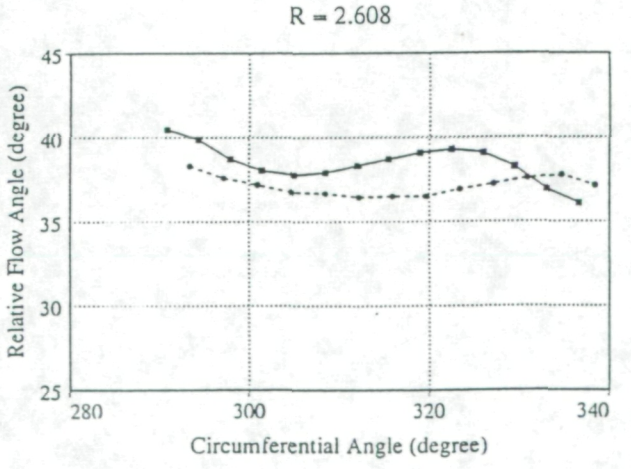
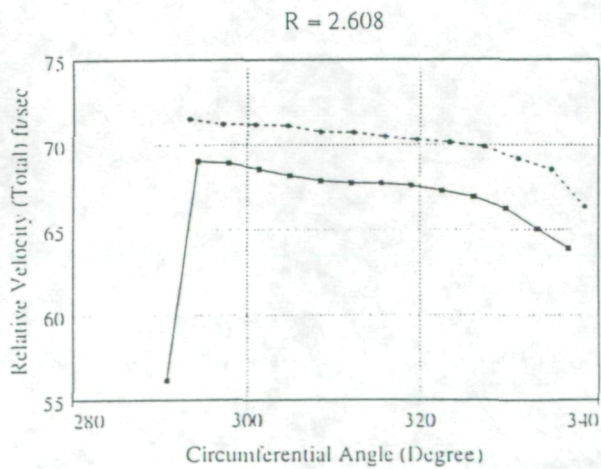
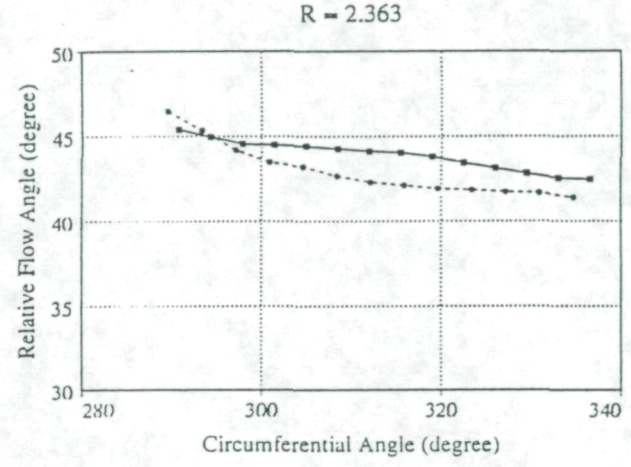
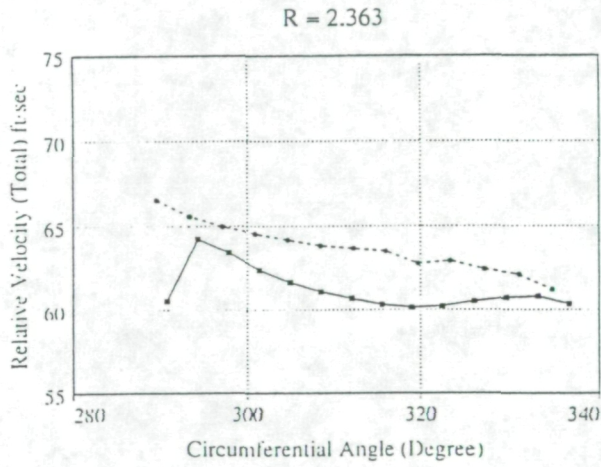
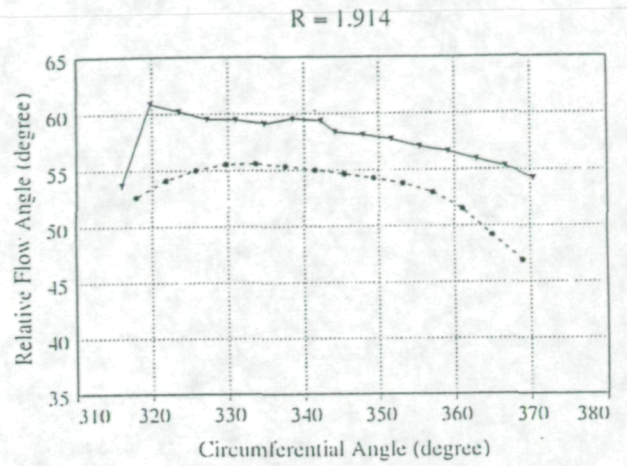
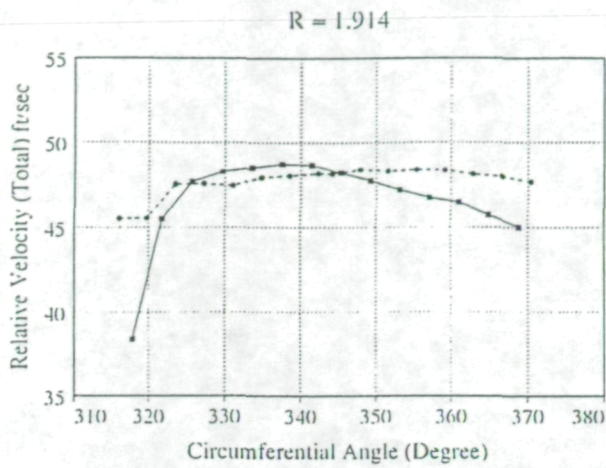


Figure 6: Comparison of relative total velocity and relative flow angle in Plane C.



Experiments  
 Computations

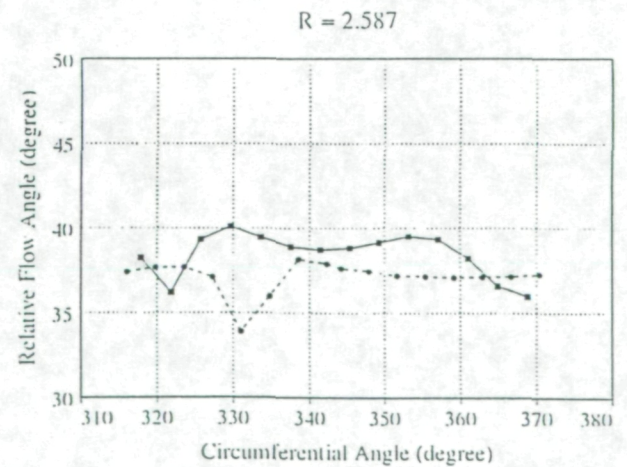
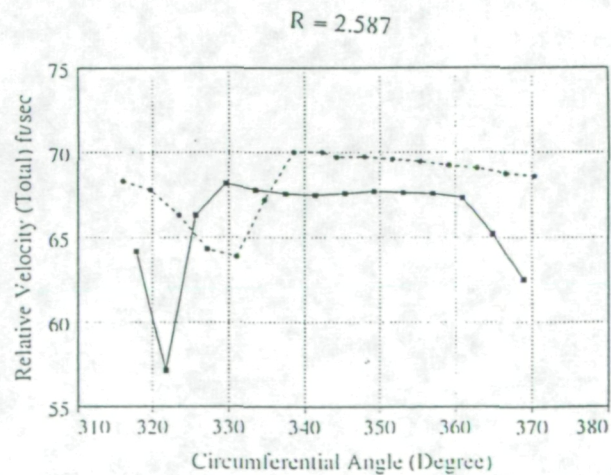
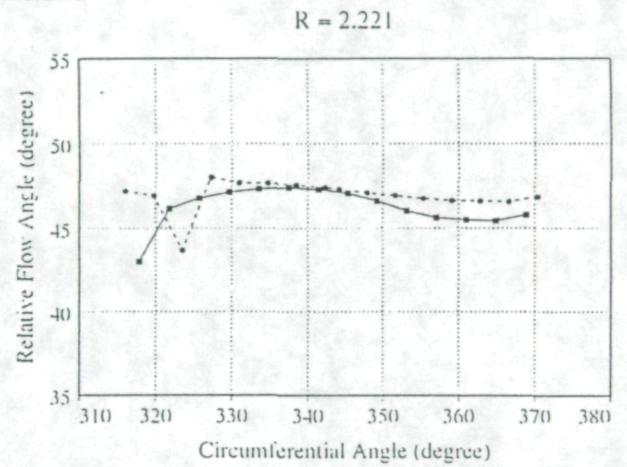
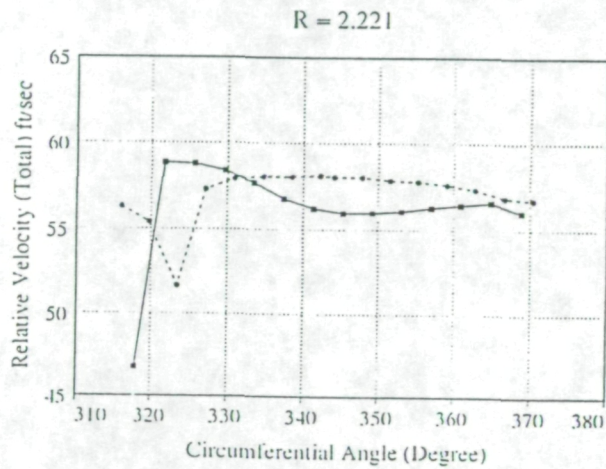


Figure 7: Comparison of relative total velocity and relative flow angle in Plane D.



Figure 8: Surface pressure for Rocketdyne inducer.



Figure 9: Velocity vectors colored by pressure on the meridional plane of the inducer.

# APPENDIX

# Computation of Incompressible Viscous Flow Through Artificial Hear Devices with Moving Boundaries

C. Kiris, S. Rogers, D. Kwak  
NASA Ames Research Center

and

I-Dee Chang  
Stanford University

Proceedings American Mathematical Society Summer Research  
Biofluidynamics Conference  
July 6-12, 1991, Seattle, WA

(To appear in ASME J. of Biofluidmechanical Engineering)